Optimisation for Optimum Nozzle Design of the Hybrid Jet-Pillar-Microchannel Heat Sink

Jyoti Pandey and Mohd. Zahid Ansari

Abstract The present study conducted an optimisation study for geometric variables of the jet nozzle of the multi-jet impingement and pillar-integrated microchannel heat sink for best performance. Nozzle diameter, nozzle angle, and nozzle diameter decreasing factor are the three design variables and minimisation of the thermal resistance is considered as the objective function. A regression model is developed using Minitab software and optimised using response surface methodology and further contribution of each variable is observed by performing analysis of variance. Nozzle angle exhibited the maximum contribution in varying the objective function that is 47.84% and thus thermal resistance was reduced by 15.8% by changing the nozzle angle from optimum conditions.

1 Introduction

Drastic escalation of temperature in the electronic component is the most concerning consequence of miniaturisation of the devices and adding up large number of functionalities in the small space with the time as it would shorten the lifespan and working efficiency of the device. Discovery of microchannel heat sink gained popularity for thermal management of high-power density micro-scale devices owing to its compact size and higher surface area to volume ratio. Tuckerman and Pease [1] corroborated that liquid-based cooling employed with microchannel can solve the future high heat dissipation problem in compact electronic devices. Numerous passive and active techniques were investigated and tested for superior hydrothermal performance of the heat sink. Techniques were focused on reducing boundary layer thickness, increasing surface area to volume ratio, improving flow mixing, inducing chaotic advection, etc. in the modified heat sink design. Jet impingement is one of the active techniques, capable of reducing boundary layer thickness, enhancing flow mixing and inducing chaos by disrupting channel flow as fluid is injected normal to

J. Pandey (✉) · Mohd. Z. Ansari
MEMS and Microfluidics Lab, Mechanical Engineering Department, PDPM Indian Institute of Information, Technology, Design, and Manufacturing, Jabalpur, MP 482005, India
e-mail: 1813602@iiitdmj.ac.in

M. A. Siddiqui et al. (eds.), *Advances in Heat Transfer and Fluid Dynamics*, Lecture Notes in Mechanical Engineering, https://doi.org/10.1007/978-981-99-7213-5_20

the surface. Higher heat transfer coefficient was achieved and hot spot was effectively treated using jet impingement in the heat sink.

Trapezoid-shaped channel surpassed circular and rectangular-shaped channel in terms of thermal performance of the microchannel heat sink with single slot jet impingement while circular channel provided highest pressure drop [2]. Lowering jet width and microchannel height contributed in decreasing surface temperature [3]. Temperature uniformity, thermal resistance and thermodynamic performance index of the channel can further be improved significantly by using multiple nozzles instead of single. Tran et al. [4] conducted study for multi-nozzle microchannel heat sink and found near to 62 and 47.3% reduction in pumping power with respect to single layer and double layer microchannel heat sink respectively. Moreover, with reducing the channel length from 10 to 1 mm, almost 62%, 10 times and 12 times improvement was obtained in thermal resistance, temperature uniformity and pressure drop respectively. Also, in case of multi-nozzle microchannel heat sink, thermal performance index and thermal resistance were improved by reducing the rib width and enlarging the channel aspect ratio.

Naphon et al. [5] investigated that approximately 18.56% heat transfer coefficient was enhanced in the microchannel heat sink by impinging jet of TiO_2 nanofluid with 0.015% concentration. Heat transfer coefficient was amplified and pressure drop was reduced even by lowering nozzle level height and increasing diameter. Mixing of spent fluid and jet of fresh fluid in case of multi-nozzle microchannel heat sink limits the cooling efficiency of the jet impingement. Also, fluid coming from the upstream nozzles obstructs the jet of fluid in the downstream region to strike directly on the bottom wall of the channel. Effusion holes were created between nozzles to limit the fluid cross-flow between neighbouring jets [6, 7].

Several hybrid multi-jet impingement microchannel heat sink flow and thermal characteristics were studied for further improvement of the microchannel heat sink performance [8, 9]. Gan et al. [10] conducted study for microchannel heat sink having jet impingement and dimples with side outlets and found improved cooling performance as well as smaller pumping power. Huang et al. [11] investigated microchannel heat sink performance for the combination of jet impingement on dimple structures of concave, convex and mixed shape. Convex dimples provided the superior overall performance as they contributed in disrupting the boundary layer whereas concave-shaped dimples provided worst performance as it created a dead zone in the flow path that blocked the fluid flow. Moreover, larger dimple radius and height provided better heat transfer performance [12, 13]. Husain et al. [13] performed numerical study for hybrid microchannel heat sink including jet impingement and pillar and found higher heat transfer coefficient for low jet pitch to jet diameter ratio and high standoff to jet diameter ratio, whereas, lower pressure drop was obtained for high jet pitch to jet diameter ratio and low standoff to jet diameter ratio.

Jet impingement heat transfer characteristic performance was significantly affected by the nozzle geometric design. Heat transfer coefficient was increased and bottom wall temperature was lowered by decreasing the size of the jet nozzle diameter along the fluid flow direction in the microchannel. However, highest temperature uniformity was obtained by using the equal size jet nozzle diameter along the length of

the microchannel heat sink. In addition, with increasing the jet nozzle diameter along the channel flow produced complex flow pattern as spent fluid flow was blocked and thus increased the temperature gradient at the bottom wall [14, 15]. Maximum wall temperature as well as thermal entropy generation rate was lowered by decreasing the jet nozzle angle against the flow direction whereas pressure drop and frictional entropy generation rate were hiked [15]. Prandtl number, Reynolds number and area ratio (ratio of total jet area and heater area) were found the influencing parameters for the heat transfer performance of the micro-jet array [16]. Strong impingement effect was obtained by reducing the jet nozzle diameter, thus bottom wall temperature was lowered while weak impingement effect was obtained with increasing the number of jet nozzles [17]. Zhang et al. [2] proposed that by optimising the single slot jet including trapezoid shaped microchannel height, bottom width and corner angle, bottom wall temperature can be reduced by 12.22, 14.85 and 7.15% respectively.

This study aimed on optimising the hybrid jet impingement and pillar included microchannel heat sink design numerically from the view of optimum nozzle geometry. Jet nozzle angle, nozzle diameter and nozzle diameter reduction factor are the three design variables chosen to be optimised. The optimisation is performed considering minimum thermal resistance as the objective function.

2 Geometric Model and Numerical Scheme

Microchannel heat sink with array of nozzle jets for impingement and pillars for flow obstruction in Fig. 1 was designed in the view of electronic cooling application. Channels of 400 μm (H_C) depth were etched on the copper substrate of 600 μm (H) height and 24 mm (L) length. Substrate total width (W) was sectioned into multiple channels of 700 μm width pitch (W_P), which is the summation of channel width (W_C) of 500 μm and substrate fin width (W_F) of 100 μm kept on each side of the channel. Circular-shaped nozzles of diameter, $D_N = 0.2$ mm, 0.25 mm and 0.3 mm were made on the glass substrate of 400 μm height (H_N) on equal distance of 2.4 mm (S). Jet of water as coolant was injected from the nozzles normal to the channel bottom surface, supplied with 100 W/cm^2 constant heat flux. After striking the bottom surface, fluid was allowed to flow parallel to the channel length in both the direction and ejected from the outlet. Circular pillars of 0.2 mm diameter (D_P) were located in between the two nozzles to act as an obstructer. To save the cost and time consumed in the numerical simulation, only half length of the single channel was considered for the computational domain shown in Fig. 2. Jet nozzle inclination angles (θ) considered in the study include $\theta = 30°, 45°, 60°$, and 90° whereas nozzle diameter was decreased along the channel length by a decreasing factor (d) from the base diameter of the nozzle (D_N) that includes $d = 0.00$ mm, 0.01 mm, 0.02 mm, and 0.03 mm.

Hybrid microchannel heat sink system with boundary conditions was simulated on the computational fluid dynamics (CFD) based commercial software Ansys FLUENT [18]. Mesh was generated with 1.3 million nodes, satisfying independency test.

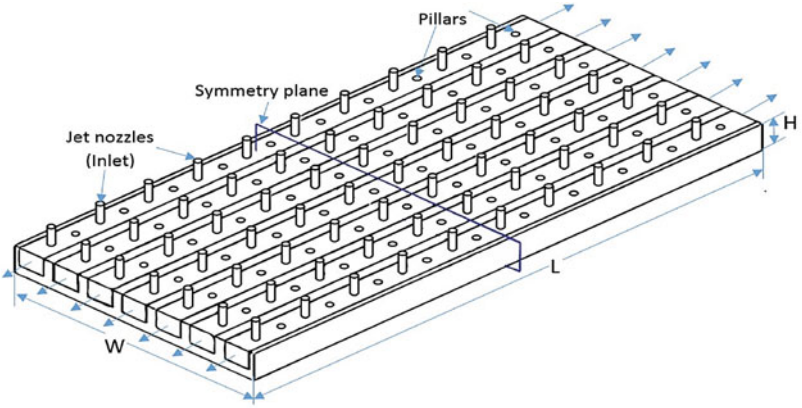

(a) Heat Sink

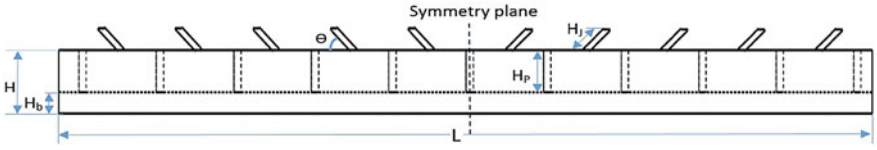

(b) Heat sink with inclined nozzles jet

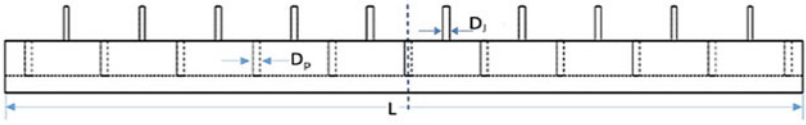

(c) Heat sink with decreasing nozzle diameter

Fig. 1 Schematic of the multiple jet impingement and pillar integrated microchannel heat sink

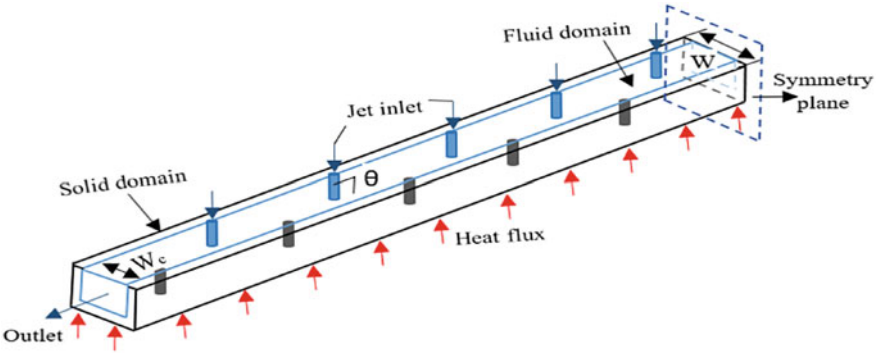

Fig. 2 Computational domain with boundary conditions of the multiple jet impingement and pillar integrated microchannel heat sink

Table 1 Properties of the solid substrate and fluid

Property	DI Water	Copper
Thermal conductivity, k (W/m^{2}K)	0.6	387.6
Specific heat capacity, C_p (J/kgK)	4182	381
Density, ρ (kg/m^3)	998.2	8978
Viscosity, μ (kg/ms)	0.001	–

Simplified fundamental governing equations such as continuity, momentum and energy were solved numerically to compute the characteristic parameters that can define the heat sink hydrothermal performance. Governing equations were simplified assuming steady state, laminar and incompressible fluid flow. In addition, fluid and substrate properties, mentioned in Table 1, were assumed independent of temperature; and radiation, viscous dissipation, and gravity effects were neglected.

Fluid domain:

Continuity equation,

$$\nabla.(\rho V) = 0 \tag{1}$$

Momentum equation,

$$V.\nabla(\rho V) = -\nabla P + \nabla.(\mu \nabla V)) \tag{2}$$

Energy equation,

$$V.\nabla(\rho C_P T) = \nabla.(k \nabla T) \tag{3}$$

Solid domain:

Energy equation,

$$\nabla.(k_{subs} \nabla T_{subs}) = 0 \tag{4}$$

Fundamental equations were discretised using second-order upwind algorithm and pressure-based solver was used for fluid flow behaviour and conjugate heat transfer analysis in the microchannel heat sink. Pressure and velocity-related variables were coupled using SIMPLE (Semi-Implicit Method for Pressure Linked Equation) scheme and residual minimisation criteria was adopted to cease the number of iterations in the numerical solution. Constant mass flow rate of fluid at a fixed temperature and uniform heat flux boundary conditions were applied at the channel inlet and bottom wall surface respectively. Channel outlets were considered to be at atmospheric boundary condition and remaining wall surfaces were considered adiabatic. No slip fluid flow condition was assumed at all the channel walls. All the boundary conditions are expressed mathematically below in Table 2.

Table 2 Boundary conditions

Boundary condition	Expression
Jet inlet	$u = u_{in}$, $v = 0$, $w = 0$, $T = T_{in}$
Outlet	$P_t = P_{atm}$, $\frac{\partial T_f}{\partial n} = 0$
Bottom surface	$-k_s \frac{\partial T_s}{\partial x} = q''$
Other walls	$\frac{\partial T_s}{\partial n} = 0$ (adiabatic), $u = v = w = 0$ (No slip)
Symmetry faces	$\frac{\partial T}{\partial n} = 0$ (adiabatic), $\frac{\partial V}{\partial n} = 0$
Solid–fluid interfaces	$k_s \frac{\partial T_s}{\partial n} = k_f \frac{\partial T_f}{\partial n}$, $T_s = T_f$, $u = v = w = 0$

3 Optimisation Methodology

Three design variables (α, δ, ϕ) were considered for the optimisation among various hybrid heat sink geometric variables from the view of designing optimum nozzle geometry. Design variables were based on changing the diameter of the nozzle, D_N; decreasing the nozzle diameter along the channel length by factor, d; changing the angle of the nozzle against the flow direction, θ. Design variables were normalised and defined while keeping the channel height (H_C) and pitch width ($W_P = W_C + W_F$; summation of channel width, W_C and fin width, W_F) constant as: α ($= D_N/W_C$) represents ratio of nozzle diameter and channel width, δ ($= d/W_C$) represents ratio of factor by which nozzle diameter was reduced along the channel length and channel width and ϕ ($= (\theta_o – \theta)/\theta_o$) represents ratio of nozzle inclination angle to the normal angle ($\theta_o = 90°$). Range of design variables chosen was $0.5 \leq \alpha \leq 0.75$, $0 \leq \delta \leq 0.075$, $0.33 \leq \phi \leq 1$. Optimisation is performed considering minimisation of the thermal resistance as objective function using polynomial-based response surface method. A second-order polynomial function is fitted between response function and design variables in the response surface approximation and applied sequential quadratic programming to search the optimal point. The mean absolute error (MAE) associated with the regression and numerical model is calculated as

$$MAE = \frac{1}{N} \sum_{i=1}^{N} \frac{\left| R_{th\_pred} - R_{th\_actual} \right|}{R_{th\_actual}} \times 100\% \tag{5}$$

The performance of the model was analysed on the basis of the minimum error and maximum correlation coefficient (R) expressed as:

$$R^2 = \frac{\sum_{m=1}^{N} \left(R_{th\_pred} - \overline{R}_{th\_pred} \right) \left(R_{th\_actual} - \overline{R}_{th\_acual} \right)}{\sqrt{\sum_{m=1}^{N} \left(R_{th\_pred} - \overline{R}_{th\_pred} \right) \sum_{m=1}^{N} \left(R_{th\_actual} - \overline{R}_{th\_actual} \right)}} \tag{6}$$

4 Results and Discussion

The numerical model is validated by the experimental work of Tuckerman and Pease [1] for fluid flow in a microchannel and Wang et al. [19] for jet impingement to ascertain the accuracy of the numerical method adopted in this study as shown in Fig. 3 and found numerical results in close proximity to the experimental results.

On-linear regression analysis is performed to develop the response model of the objective function, R_{th} using minitab [20] in terms of normalised nozzle geometric variables that is α, δ and ϕ as shown below:

$$R_{th} = 1.232 + 6.691 \times \alpha + 0.754 \times \phi + 7.34 \times \delta - 5.341 \times \alpha \times \phi - 43.3 \times \alpha \times \delta + 15.10 \times \phi \times \delta \quad (7)$$

The correlations formulated are applicable for water as coolant in the jet impingement pillar-integrated microchannel heat sink with normalised nozzle geometric variables within a specified range of $0.5 \leq \alpha \leq 0.75$, $0 \leq \delta \leq 0.075$, $0 \leq \phi \leq 0.6667$. Empirical relations predicted values of Rth are compared with the actual numerical data as shown in Fig. 4. Predicted Rth data values at the most deviate from the actual value by $\pm$ 6.5%, R^2 and MSE error associated with the R_{th} is 94.30% and 2.898% respectively.

Analysis of Variance (ANOVA) was performed as presented in Table 3 to find the relative contribution of each geometric design variable. It is found that ϕ exhibits the maximum contribution that is 47.84% on affecting the objective function followed by α having 26.97%, and least contributed by δ that is 14.50%. Figure 5 and Fig. 6 showed the effect of each design variable and their interaction on the objective function for the better cooling performance of the MJI-P-MCHS. It is found from Fig. 5 that the mean of the objective function value is continuously increasing with increasing the α that means thermal resistance will be higher for larger diameter of

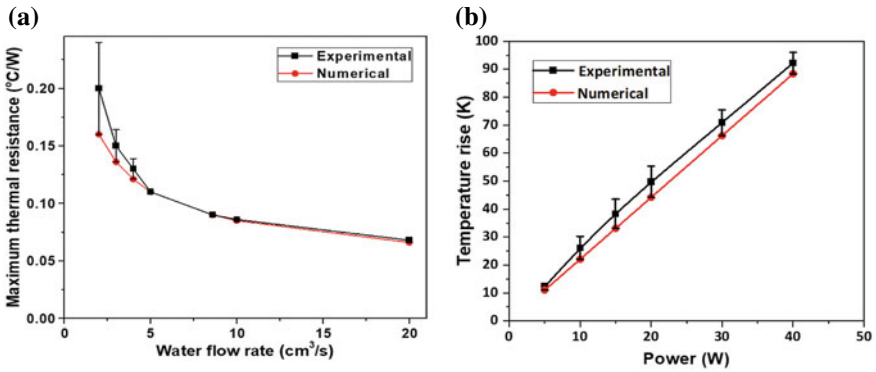

Fig. 3 The numerical and experimental results are compared to validate the numerical model for **a** microchannel heat sinks [1] and **b** jet impingement techniques [19]

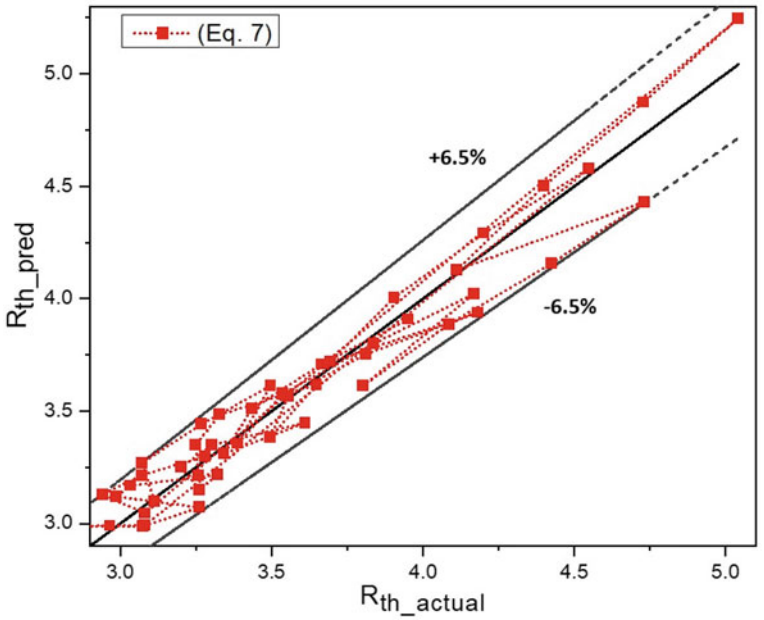

Fig. 4 Comparison of the actual and predicted value of the thermal resistance

the jet which is attributed to the smaller velocity of the jet impinged from the larger size nozzle. Similarly, mean of the objective function value continuously increased as the ϕ increases that means thermal resistance will be higher for larger angle of the jet which is attributed to the smaller path length of the jet in the fluid domain. In addition, mean of the objective function value decreased fast as the δ increased but later on slow down after 0.04 that means thermal resistance will be higher for equal diameter of the jet along the length while it is reduced with deceasing the jet diameter along the flow which is attributed to the enhanced flow mixing by higher velocity jet impinged by the smaller diameter nozzle in the downstream. Interaction plots in Fig. 6 presented that for constant δ, objective function mean value is lower for smaller value of the α and larger value of ϕ. In addition, for constant ϕ, objective function mean value is lower for smaller value of the α but larger value of the δ for higher α whereas for smaller α, objective function mean value first decreased and then increased with increasing the δ. Similarly, for constant α, objective function mean value is lower for larger value of the ϕ but larger value of the δ for higher ϕ whereas for smaller ϕ, objective function mean value first decreased and then increased with increasing the δ.

Regression equation is optimised for the minimum R_{th} and found optimum value as $R_{th} = 2.965 \times 10^{-3}$ W/K at $\alpha = 0.4$, $\phi = 0.667$, and $\delta = 0.04$. Furthermore, variation in R_{th} is observed by changing the design variables from optimum condition as presented in Fig. 7. R_{th} was reduced by 8.3, 15.8 and 3.5–3.7% by changing the α from 0.4 to 0.6, ϕ from 0.667 to 0 and δ from 0.04 to 0 or 0.06 respectively.

Table 3 ANOVA of each design variable

Design variable	Seq SS	Contribution (%)
α	3.690	26.97
ϕ	6.545	47.84
δ	1.984	14.50
Error	1.463	10.69
Total	13.681	100.0%

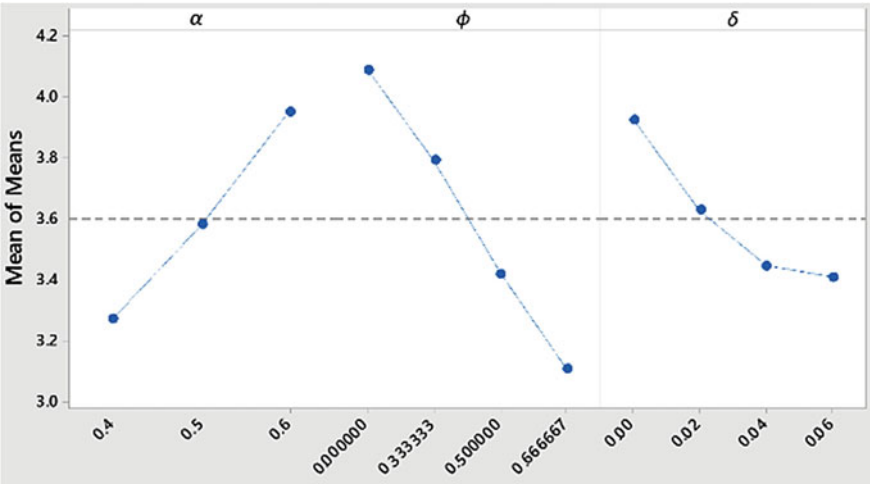

Fig. 5 Main effect plots for the means of the objective function for each design variable

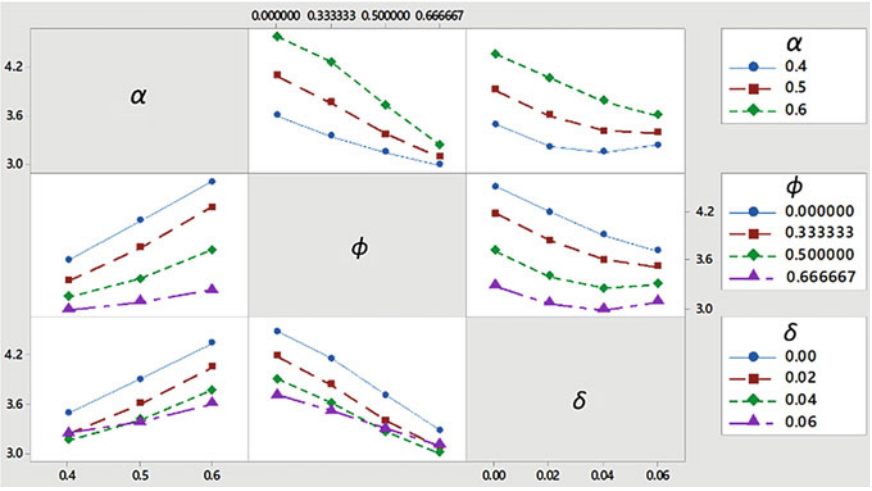

Fig. 6 Interaction plots for the means of the objective function for each design variable

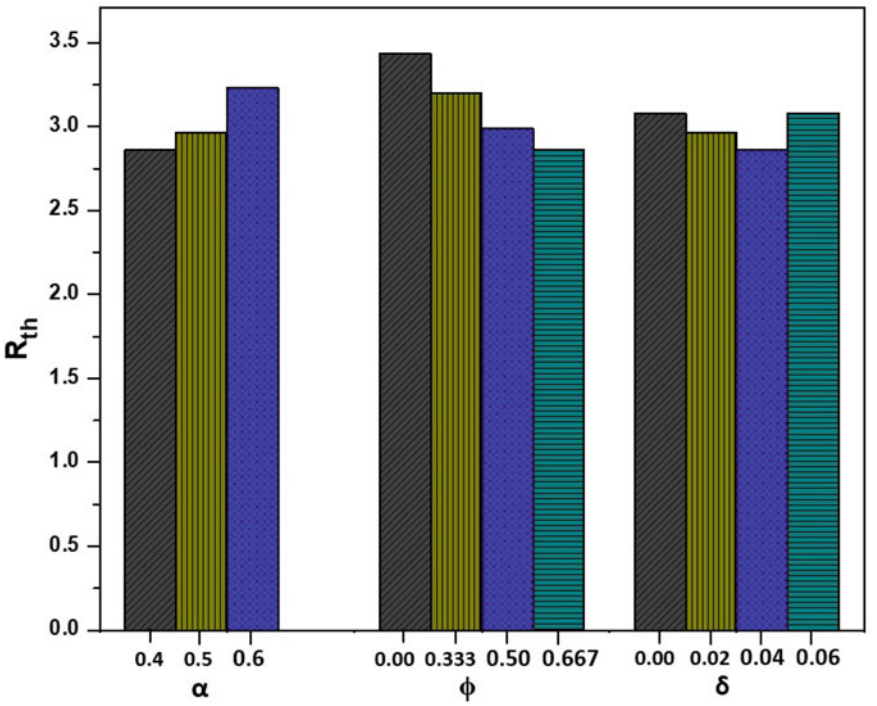

Fig. 7 Comparison of thermal resistance change for design variables deviating from the optimum value

5 Conclusion

An optimisation study was performed using the data obtained from numerical analysis for the performance improvement of the hybrid multiple micro-jet and pillar-integrated microchannel heat sink. Minimum thermal resistance was chosen as the objective function and normalised jet nozzle geometric variables such as nozzle diameter, nozzle angle, and nozzle diameter decreasing factor were considered as design variables. An improvement was observed by changing the design variables value and maximum contribution that is 47.84% was given by the nozzle angle followed by nozzle diameter and least by the nozzle diameter decreasing factor. Moreover, a reduction of 15.8% was observed by decreasing the nozzle angle from optimum condition.

Acknowledgements This work was supported by IIITDM Jabalpur, India.

References

1. Tuckerman DB, Pease RFW (1981) IEEE Electron Device Lett. EDL-2(5):126–129
2. Zhang Y, Wang S, Ding P (2017) Int J Heat Mass Transf 113:295–309
3. Sung MK, Mudawar I (2006) Int J Heat Mass Transf 49:682–694
4. Tran N, Chang Y-J, Teng J-T, Dang T, Greif R (2016) Int J Heat Mass Transf 101:656–666
5. Naphon P, Nakharintr L, Wiriyasart S (2018) Int J Heat Mass Transf 126:924–932
6. Husain A, Ariz M (2017) Int J Engg 30(10):1599–1608
7. Husain A, Al-Azri NA, Al-Rawahi NZH (2015) J Thermophys Heat Transf 30(2):1–7
8. Pandey J, Husain A, Ansari MZ (2022) Proc IMechE Part C J Mech Eng Sci 236 (17):9814–9827
9. Pandey J, Ansari MZ, Husain A (2021) Int J Num Methods Heat Fluid Flow 32(8):2659–2681
10. Gan T, Ming T, Fang W, Liu Y, Miao L, Ren K, Ahmadi MH (2020) J Thermal Anal Calorimetry 141:45–56
11. Huang X, Yang W, Ming T, Shen W, Yu X (2017) Int J Heat Mass Transf 112:113–124
12. Tingzhen M, Cunjin C, Wei Y, Wenqing S, Wei F, Nan Z (2018) J Therm Sci 27(3):321–330
13. Husain A, Ariz M, Al-Rawahi NZH, Ansari MZ (2016) Appl Therm Engg 102:989–1000
14. Sung MK, Mudawar I (2008) Int J Heat Mass Transf 51:4614–4627
15. Pandey J, Ansari MZ, Husain A (2021) J Mech Sci Tech 35(12):5753–5764
16. Michna GJ, Browne EA, Peles Y, Jensen MK (2011) Int J Heat Mass Transf 54:1782–1790
17. Kim SH, Shin H-C, Kim S-M (2019) J Mech Sci Tech 33(7):3555–3562
18. ANSYS Fluent (2017) version 18.0, Canonsburg, PA, US
19. Wang EN, Zhang L, Jiang L, Koo J-M, Maveety JG, Sanchez A, Goodson KE, Kenny TW (2004) J Microelectromech Syst 13(5):833–842
20. Ryan BF, Ryan TA Jr, Joiner BL (2017) Minitab, version 18. PA, US